IIETA International Information and Engineering Technology Association
Advancing the World of Information and Engineering

Journal Européen des Systèmes Automatisés
Vol. 59, No. 3, March, 2026, pp. 825-837
Journal homepage: http://iieta.org/journals/jesa

Design and Controlled-Environment Evaluation of a Portable Depth-Aware Prototype for Multi-Parameter Water Quality Profiling

Moh. Eldivo Alsyawal Otoluwa[1], Aswangga Pandita Sadu[1], Muh. Fathir Qinthara[1], Muhammad Akmal Falih Rizqulla[1], Mikhail Sannata Widjaya[1], Luthfi As-Sidq[1], Istiqomah[1,2*], Fiky Yosef Suratman[1,2]

[1] School of Electrical Engineering, Telkom University, Bandung 40257, Indonesia
[2] The University Center of Excellence Intelligent Sensing-IoT, Telkom University, Bandung 40257, Indonesia

Corresponding Author Email: Istiqomah@telkomuniversity.ac.id

https://doi.org/10.18280/jesa.590324

Received: 6 January 2026
Revised: 12 March 2026
Accepted: 22 March 2026
Available online: 31 March 2026

Keywords:
controlled-environment validation, depth-aware profiling, inland waters, Internet of Things, portable prototype, water quality monitoring

ABSTRACT

This study presents the design, calibration, and controlled-environment evaluation of a portable depth-aware water-quality monitoring prototype intended to improve observation of vertical water-quality variation in inland waters. The system integrates a floating supervisory and actuation unit, a submersible sensing unit, and an Internet of Things (IoT)-based communication and visualization layer to measure temperature, pH, dissolved oxygen (DO), turbidity, and depth at user-requested positions. Controlled calibration showed mean post-regression errors of 0.10% for temperature, 1.12% for pH, 0.58% for depth, and 4.80% for DO. Evaluation in a 4-m pool produced coherent multi-parameter measurements in a nearly homogeneous water column, confirming null-profile consistency. Depth-positioning tests showed the largest error at the 50-cm setpoint (8–10 cm), while deeper setpoints between 100 and 400 cm showed smaller deviations. End-to-end IoT validation confirmed consistent local display, cloud storage, and mobile access, and LoRa testing showed 0% packet loss up to 70 m under line-of-sight conditions. These results support controlled-environment prototype feasibility and provide a basis for future, longer-term inland-water monitoring of depth-dependent water-quality gradients.

1. INTRODUCTION

Lakes and reservoirs provide essential services related to water supply, irrigation, fisheries, hydropower, and ecosystem regulation. At the same time, they are highly responsive to climate variability, land-use change, and pollutant loading, making them sensitive indicators of environmental degradation and water-security risk [1-3].

In inland waters, water quality often varies not only across location but also with depth. Vertical gradients in temperature, dissolved oxygen (DO), and other physicochemical parameters are especially important in stratified lakes and reservoirs, where surface-only observations may fail to represent subsurface or bottom-water conditions. In tropical systems, prolonged stratification can promote oxygen depletion, internal loading, and rapid deterioration of ecological conditions, while studies in Indonesian lakes have highlighted the importance of vertical structure and the risk of hypolimnetic anoxia in deep tropical waters [4, 5].

Conventional monitoring in many inland-water settings still relies on grab sampling, bottle-based depth sampling, or limited surface measurements. Although such approaches can provide useful point observations, they are weak in temporal continuity and vertical resolution. In addition, when water samples are collected manually at depth and then brought to the surface for later analysis, part of the practical advantage of direct in-situ observation is lost because the measurements are no longer obtained immediately at the target layer. This limitation becomes critical when water quality changes with depth, because important deterioration processes may remain undetected when only near-surface observations or delayed sample analysis are available. Indonesian regulatory standards, including PP No. 22/2021, also require evaluation of core water-quality parameters such as temperature, pH, DO, and turbidity, which further motivates more practical and informative monitoring strategies for lakes and reservoirs [6].

Recent work has shown that high-frequency in-situ monitoring can substantially improve the observation of rapid ecological and physicochemical changes in lakes and reservoirs, thereby supporting more responsive environmental assessment and management. Automated monitoring approaches are increasingly recognized as valuable tools for resolving short-term fluctuations, seasonal transitions, and episodic events that are often missed by conventional low-frequency sampling. This need is especially relevant for DO, which is a critical water-quality parameter and whose systematic and continuous monitoring is important where environmental conditions are prone to fluctuation [7-11].

Recent developments in embedded electronics and Internet-of-Things (IoT) systems have enabled a growing number of low-cost water-quality monitoring platforms with real-time sensing and remote data access. However, many existing low-cost systems remain fixed in position, operate primarily at the surface, or are designed for rivers, shallow deployments,

point-of-use testing, or offshore aquaculture rather than portable inland-water profiling. For example, previous studies have reported compact and practical surface-based multiparameter sensing systems [11, 12], highlighted the feasibility of long-term low-cost monitoring [13], and presented a buoy platform intended for offshore aquaculture applications [14]. Despite these advances, a practical gap remains between low-cost surface-monitoring systems and portable platforms capable of collecting depth-resolved profiles in inland lakes and reservoirs.

This study addresses that gap through the development of a depth-aware water-quality monitoring prototype integrating three main subsystems: a floating supervisory and actuation unit, a submersible sensing unit, and an IoT-based communication and visualization layer. The proposed system combines multi-parameter sensing with winch-based vertical positioning and cloud/mobile data access so that water-quality observations can be associated with measurement depth rather than being limited to the water surface. More specifically, the practical contribution of this work lies in enabling direct in-situ measurement at user-requested depths and returning those depth-associated measurements through an integrated real-time monitoring workflow. The technical contribution of this work is therefore not the introduction of a new sensing principle, but the engineering integration of vertical profiling capability, floating and submersible subsystems, and IoT-enabled data handling within a portable monitoring architecture intended for inland waters.

The scope of the present paper is limited to controlled-environment prototype validation. The system is calibrated and evaluated in a 4 m pool to assess sensor performance, depth-positioning behavior, multi-depth measurement consistency, and end-to-end IoT functionality. Accordingly, the study should be interpreted as a prototype feasibility study for future lake and reservoir deployment rather than as a fully field-validated monitoring solution.

2. METHODOLOGY

2.1 System architecture and operational logic

The proposed water-quality monitoring prototype was implemented as an integrated system composed of three main subsystems: a submersible sensing unit, a floating supervisory and actuation unit, and an IoT-based communication and visualization system. In the realized prototype, the submersible unit performs direct in-water measurements of temperature, pH, turbidity, DO, and depth, while the floating unit regulates the vertical position of the sensing module and serves as the main supervisory controller. The IoT subsystem provides the user interface, stores measurement requests and results in the database, and supports remote visualization of measurement data.

The architectural relationships among the main components are illustrated in Figure 1. As shown in Figure 1(a), the system receives user-requested measurement depth, measurement-location information, water input, and power supply, and produces measurement results together with depth-level information for user access. Figure 1(b) further highlights the internal role of the floating unit as the supervisory subsystem that integrates coordinate detection, the control unit, the communication module, and the pulley actuator, while also receiving depth and water-quality data from the submersible unit. In this arrangement, the floating unit acts as the interface between underwater sensing, local actuation, and remote communication.

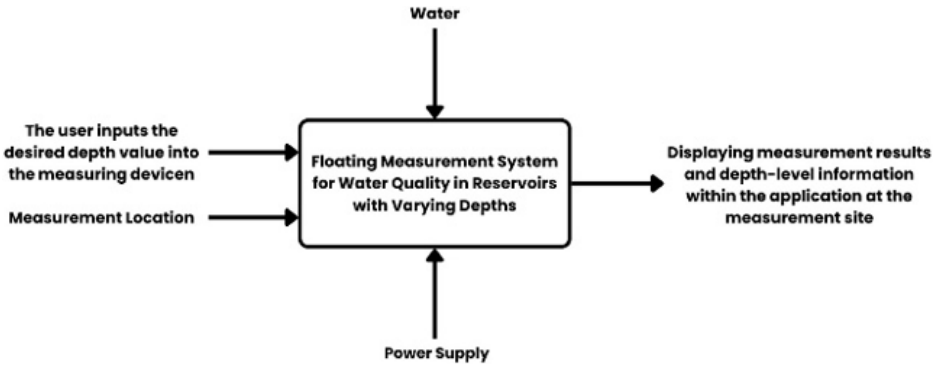

(a) Overall block diagram

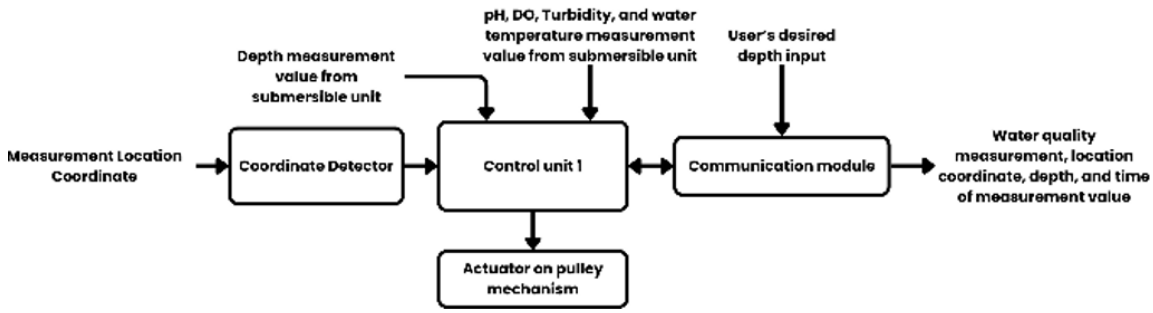

(b) Floating system unit diagram

Figure 1. System architecture diagrams

Operationally, the user enters one or more requested depths through the application interface. These commands are stored in the cloud database, relayed by the gateway, and transmitted to the floating unit through the wireless link. The floating unit

then acquires the measurement coordinates, regulates the submersible unit to the requested depth, receives the measured water-quality data, and forwards the results for storage and user access. The returned records include the measured parameters together with associated depth, location, and time metadata.

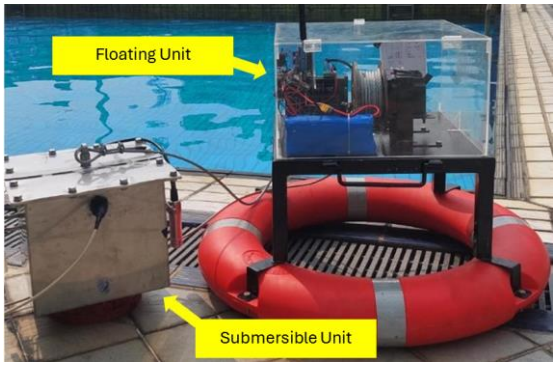

Figure 2. Realized prototype

Figure 2 shows the realized prototype of the integrated monitoring system, including the floating and submersible units. The operational sequence of this prototype is presented in Figure 3, which demonstrates how user commands are received, the sensing unit is positioned to the requested depth, measurements are acquired in situ, and the resulting data are returned through the same integrated monitoring chain.

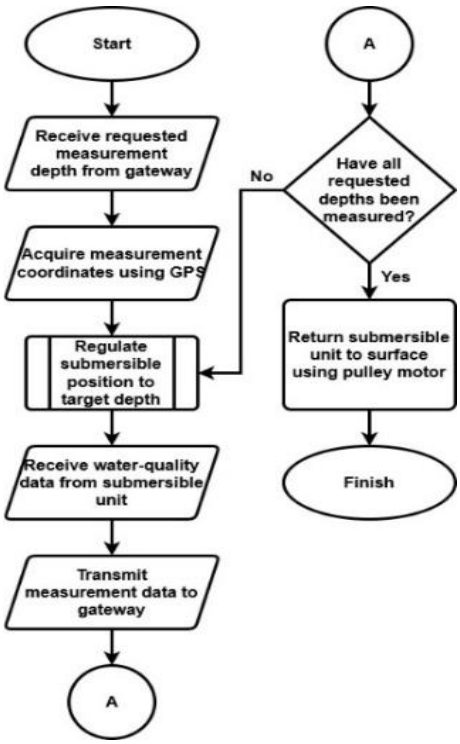

Figure 3. Overall operational flow

2.2 Depth positioning and regulation system

The platform performs multi-depth measurements by regulating the vertical position of the submersible unit using a pressure-based depth estimate and a pulley-driven actuation mechanism. Depth is determined from a hydrostatic pressure sensor mounted on the submersible unit. In the realized prototype, depth is estimated from the hydrostatic pressure difference between the submerged pressure sensor and the reference pressure near the surface, following:

$$\Delta P = \rho g h \tag{1}$$

so that

$$h = \frac{\Delta P}{\rho g} \tag{2}$$

This pressure-based depth estimate was then calibrated experimentally in a 4 m water column before being used as feedback for position regulation.

Depth regulation was implemented as a rule-based feedback routine. After the floating unit receives a requested measurement depth from the gateway, it periodically receives the actual depth of the submersible unit from the pressure-sensor data and compares this value with the requested setpoint. If the submersible unit is shallower than the requested depth, the floating-unit controller commands the actuator to release the cable so that the sensing unit moves downward. If the submersible unit is deeper than the requested depth, the controller commands the actuator to retrieve the cable so that the sensing unit moves upward. This comparison-and-correction process is repeated until the target position is reached, after which the sensing sequence is initiated.

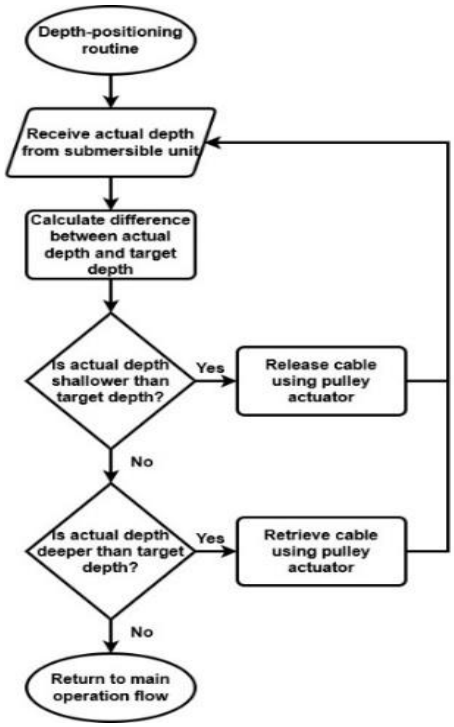

Figure 4. Rule-based depth-positioning routine

The rule-based depth-positioning logic implemented on the floating unit is shown in Figure 4. As illustrated in the flowchart, the system repeatedly receives updated depth information from the submersible unit, calculates the difference between actual depth and target depth, and applies directional correction through the pulley actuator. In this sense, the present design should be interpreted as a practical depth-regulation mechanism based on hydrostatic feedback and cable actuation, rather than as a fully tuned high-order control system.

The depth-positioning mechanism is physically implemented through a stepper-motor-driven pulley located on the floating unit. The pulley winds or unwinds the suspension cable connected to the submersible unit, thereby controlling the probe position within the water column. This architecture allows the positioning task to remain on the floating unit while the submersible unit focuses on sensing and depth feedback. Once the requested depth has been reached, the submersible unit acquires the water-quality parameters and returns the measurement data to the floating unit. If additional target depths remain, the same positioning-and-measurement sequence is repeated for the next requested setpoint. After all requested depths have been measured, the floating unit returns the submersible unit to the surface. The experimental performance of this depth-positioning mechanism is evaluated separately in Section 3.3.

2.3 Submersible unit design and sensor integration

The submersible unit was implemented as the in-water sensing subsystem responsible for measuring temperature, pH, turbidity, DO, and depth at user-requested positions within the water column. In the realized prototype, all sensing components were integrated into a stainless-steel enclosure with approximate dimensions of 22 × 22 × 25 cm and a total submersible-unit mass of about 15 kg. The enclosure was equipped with a top attachment point for connection to the floating unit through the suspension cable, allowing the sensing module to be lowered and raised during profiling operation. This realized design functions as the main housing for the underwater sensing and local processing components.

The sensing elements installed on the submersible unit are summarized in Table 1, which lists the measured parameters, sensor types, operating ranges, nominal accuracy, and output interfaces used in the realized prototype. The implemented sensor set consisted of a DS18B20 temperature sensor, an Atlas Scientific pH probe, a DFRobot DO sensor, a DFRobot turbidity sensor, and an XIDIBEI XDB500 pressure sensor for depth estimation. In this arrangement, the pressure sensor serves a dual role: it provides the depth-feedback signal required for vertical positioning and also supplies the depth metadata associated with each water-quality measurement.

Table 1. Technical specification

Parameter	Sensor	Range	Accuracy	Output
Temperature	DS18B20	10–50 °C	± 0.5 °C	Digital
pH	Atlas Scientific	0–14	± 0.01	Analog
Dissolved Oxygen (DO)	DFRobot DO Sensor	0–20 mg/L	± 0.2 mg/L	Analog
Turbidity	DFRobot Turbidity Sensor	0–1000 NTU	± 5 %	Analog
Depth	XIDIBEI XDB500	0-300 m	± 0.5%	Analog

Within the submersible unit, the sensors were interfaced to an Arduino Mega 2560, which served as the local controller for data acquisition and transmission to the floating unit. The realized wiring arrangement of this subsystem is shown in Figure 5. As indicated by the wiring diagram, the water-quality sensors were read through the submersible controller, while the pressure sensor required a higher supply voltage and was therefore supported by the power subsystem on the floating unit. This arrangement allowed the submersible unit to act as a dedicated underwater acquisition module while remaining electrically integrated with the surface supervisory unit. The sensing and data-acquisition sequence executed by the submersible unit is summarized in Figure 6.

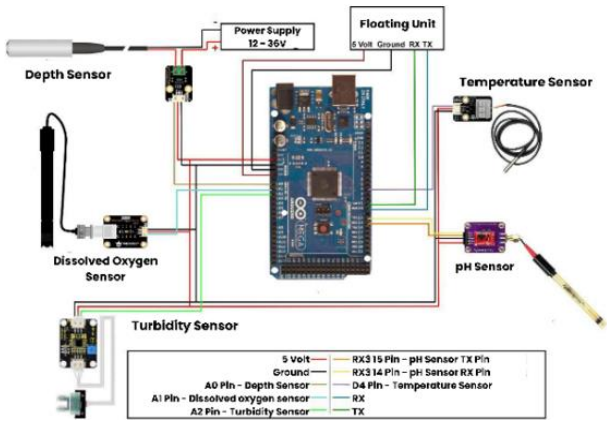

Figure 5. Wiring of submersible unit

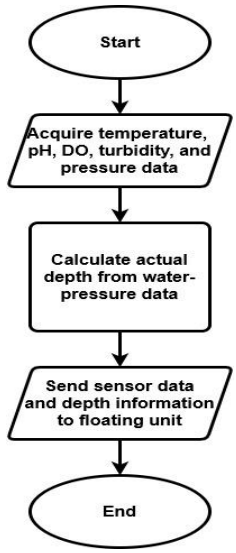

Figure 6. Submersible sensing and data-acquisition flow

Sensor selection was based on the need to measure the core water-quality parameters of interest while maintaining compatibility with submerged operation to approximately 4 m depth under controlled test conditions. The pH probe had a pressure and depth specification well above the tested range, and the pressure sensor provided the clearest underwater operating specification through its protected submersible construction. The DO probe also produced usable output during fully submerged 4 m pool testing, although its practical behavior was less stable than the other sensing channels, as discussed later in Section 3.1.

Sensor suitability was not uniform across all channels. In particular, the turbidity sensor did not include an off-the-shelf waterproof specification for full immersion, so sealing was applied to the probe gaps to allow controlled pool testing. At the enclosure level, sealed cable-entry points were used to support underwater operation. Waterproof testing showed no leakage at 1–2 m, but slight seepage was still observed at 3–4 m, most likely because small cable-entry gaps were not fully closed despite silicone sealing. Accordingly, the submersible

unit should be interpreted as a practical prototype enclosure for controlled testing rather than a fully field-hardened underwater package. This limitation is also consistent with broader experience in low-cost turbidity instrumentation, where waterproofing, continuous in-situ operation, compactness, and cost remain important tradeoffs [15-17].

2.4 Floating unit design and integration

The floating unit was implemented as the supervisory and actuation subsystem of the prototype. Its primary functions were to regulate the vertical motion of the submersible unit, receive measurement data from the submerged sensing module, acquire supporting metadata such as geographic position, and forward the resulting dataset for storage and user access. In the realized implementation, this subsystem therefore served as both the local controller and the communication interface between the submersible unit and the IoT layer. The hardware configuration of the floating unit consisted of a microcontroller, stepper motor, motor driver, wireless communication module, GPS module, display interface, and power subsystem. The realized wiring arrangement of these components is shown in Figure 7. In the implemented circuit, the main supply stage provided approximately 27 V, which was stepped down to 5 V to match the operating requirements of the control and communication electronics.

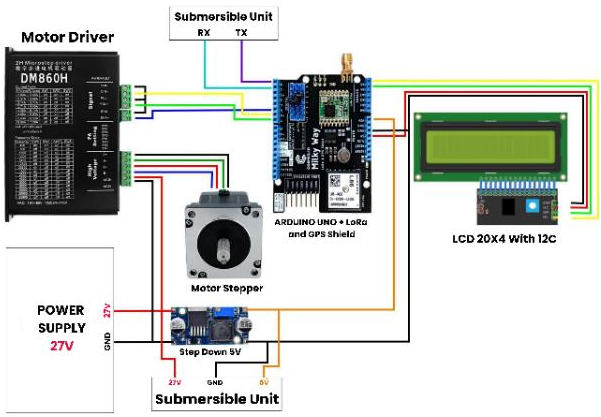

Figure 7. Wiring of the floating unit

Mechanically, the floating unit regulates depth through a shaft-and-cable arrangement driven by the stepper motor. The suspension rope was wound directly on the actuator shaft, and vertical motion of the submersible unit was achieved by releasing or retrieving the cable according to the requested depth. In the design-selection stage, Dyneema rope was chosen as the pulling medium because of its favorable durability and tensile-strength characteristics relative to the other evaluated options. This arrangement allows the floating unit to retain the actuation function at the surface while the submersible unit remains dedicated to sensing and depth feedback.

A practical basis for actuator selection was established through both component comparison and first-order mechanical estimation. In the motor-selection stage, the compared criteria were price, torque, current requirement, and weight, with torque assigned the greatest weight (40%) because the motor was required to pull and release the cable connected to the submersible unit. Based on this comparison, the selected actuator was a NEMA 34 stepper motor with nominal torque of 4.5 Nm. To support this choice, a simple buoyancy-based load estimate and a corresponding shaft-torque calculation were performed using the realized dimensions and mass of the submersible unit. The calculation is provided below.

Given:

- Submersible unit dimensions: $l \times w \times H = 22 \times 22 \times 25\ cm$
- Submersible unit mass: $m = 15\ kg$
- Shaft radius: $r = 20\ mm = 0.02\ m$
- Water density: $\rho = 1000\ {}^{kg}/_{m^3}$
- Gravitational acceleration: $g = 9.81\ {}^{m}/_{s^2}$

Displaced volume

$$V = lwH \tag{3}$$

Buoyant force

$$F_b = \rho g V \tag{4}$$

Dry weight of submersible unit

$$W = mg \tag{5}$$

Estimated net submerged force

$$F_{net} = W - F_b \tag{6}$$

Minimum shaft torque

$$T = F_{net} \bullet r \tag{7}$$

Using the realized prototype dimensions and mass, the calculation yields a first-order estimate of 28.449 N for the net submerged force and approximately 0.57 N·m for the minimum shaft torque. Although this result is only an engineering estimate, it remains substantially below the rated torque of the selected 4.5 N·m stepper motor and therefore supports the actuator choice for the present prototype.

The actuator choice was also supported experimentally through stepper-motor lifting tests. In these tests, the motor was required to lift a 12.5 N load over an 85 cm travel distance at multiple step-per-revolution settings (800, 6400, and 8000). All tested settings were able to lift the load successfully, while lower step-per-revolution settings produced faster movement and higher settings provided finer positioning at the expense of slower motion. This behavior supported the adoption of stepper-driven cable actuation for depth regulation in the floating supervisory unit.

From a buoyancy perspective, the floating unit was mounted on a buoyant frame constructed from lightweight PVC and foam elements to support surface operation and protect the electronics from splash exposure during testing. In the original design stage, buoyancy and stability were considered using an intended mass target of 16.4 kg. However, subsequent prototype realization required additional reinforcement and ballast-related adjustments at the system level, so the present study should interpret the floating platform as a realized prototype surface support structure rather than as a fully weight-optimized final design. In practical terms, the floating platform had to provide sufficient support for the controller, actuator, communication, GPS, and

power subsystems while maintaining stable operation above the water surface, whereas the submerged unit was deliberately given negative buoyancy to support underwater positioning.

Overall, the realized floating unit should be understood as a prototype supervisory platform that combines depth actuation, communication, localization, and power management in a single surface-mounted subsystem. Its main engineering role is to connect user-requested depth commands, underwater sensing, and wireless data transmission in one integrated system. The experimental performance of its depth-positioning and communication functions is evaluated separately in Sections 3.3 and 3.4.

2.5 Sensor calibration protocol

All sensors were calibrated under controlled conditions prior to integrated system validation. For each calibration sample or reference condition, repeated sensor readings were acquired and averaged before regression-based correction was applied. The resulting calibration equations were then embedded in the firmware so that raw sensor outputs could be converted into compensated physical units during system operation. In the present calibration procedure, temperature and pH calibration points were each averaged from 30 repeated readings, while turbidity and depth-pressure calibration points were averaged from 20 repeated readings before regression analysis. DO calibration was carried out using the same controlled-regression approach, with the reference concentrations taken from the calibration set described below. This distinction between regression-based calibration adequacy and longer-term operational qualification is also consistent with recent discussions on water-quality sensor evaluation, which emphasize that calibration performance should be interpreted together with repeatability, stability, and suitability for the intended monitoring context [18, 19].

Temperature calibration was performed using multiple water samples referenced by a laboratory thermometer, with four calibration points spanning 20.00, 25.00, 37.50, and 40.00 °C. The pH sensor was calibrated using four standard buffer conditions covering acidic to alkaline values, namely pH 4.00, 7.00, 9.26, and 9.50. DO calibration used a portable reference meter over four concentrations between 0.00 and 5.80 mg/L. For turbidity calibration, water samples with different turbidity levels were first measured using a reference turbidimeter and then compared against the sensor output; three reference levels were used in the present prototype calibration, namely 3.37, 78, and 664 NTU. Depth calibration was conducted separately using the hydrostatic pressure sensor in a 4 m water column, with eight known reference depths between 500 and 3900 mm.

Linear or polynomial regression models were selected according to the response characteristics of each sensor and used as the basis for firmware-level compensation. For temperature, pH, DO, and depth, calibration performance is reported in Section 3.1 using post-regression percentage error. For turbidity, calibration performance is reported using absolute residuals in NTU rather than percentage error, because the reference values are expressed directly in physical turbidity units and residuals in NTU provide a more interpretable measure of deviation over the tested points.

The present calibration campaign was intended to support controlled prototype validation rather than full long-term field qualification. Calibration density was not uniform across all channels: the temperature, pH, and DO sensors each used four reference points, turbidity used three, and the depth sensor used eight. Accordingly, these calibration results should be interpreted as sufficient for controlled-system evaluation, while broader calibration coverage and long-duration drift assessment remain necessary for future field deployment studies. More generally, the distinction between prototype calibration and operational monitoring readiness has long been recognized in water-quality assessment and monitoring practice [20-22].

2.6 IoT system design

The IoT subsystem was implemented to support remote command entry, data transmission, cloud storage, and user-side visualization of the measured water-quality parameters. In the realized prototype, this subsystem consisted of a mobile application, a Firebase Firestore cloud database, a gateway device, and the floating measurement unit connected through LoRa communication. Rather than functioning only as a passive display layer, the IoT subsystem also served as the command path through which the requested measurement depths were delivered to the floating unit.

Operationally, the user enters one or more requested measurement depths through the mobile application, and these values are stored in Firebase Firestore as the command source for the system. The gateway monitors the database for updated requests and transmits valid commands through LoRa to the floating unit, which then performs the depth-positioning and sensing sequence. After measurement, the resulting water-quality data are returned through the same communication chain and stored in the database for display in the application. This end-to-end communication workflow of the implemented IoT subsystem is illustrated in Figure 8.

Firestore was selected because its document-based structure supports storage of multi-parameter measurements together with associated depth, timestamp, and location metadata. In the realized implementation, the gateway also parsed incoming LoRa payloads and wrote the processed values to the database, which simplified synchronization with the application.

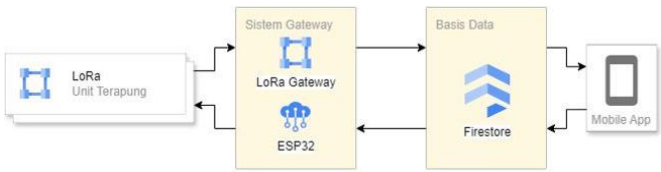

Figure 8. IoT system communication flow diagram

The mobile application consisted of Home, Maps, and History pages. Home was used for depth entry, Maps for location-linked visualization of completed measurements, and History for chronological review of stored records. In this way, the IoT subsystem served as an integrated command, storage, and visualization layer rather than merely a cloud logging add-on. This architecture is consistent with the broader development of IoT-based water-quality monitoring systems, which increasingly emphasize real-time data access, cloud-connected logging, and remote user interaction as core functions of practical environmental monitoring platforms [23, 24]. Its communication reliability and data consistency under the reported test conditions are evaluated in Section 3.4.

3. RESULTS AND DISCUSSION

3.1 Sensor calibration and accuracy assessment

All sensors were calibrated under controlled conditions prior to integrated system validation, and the resulting compensation functions were embedded in the firmware as described in Section 2.5. For each calibration point, repeated readings were acquired and averaged before regression-based correction was applied. In the present calibration procedure, temperature and pH calibration points were each based on 30 repeated readings, while turbidity, DO, and depth-pressure calibration points were based on 20 repeated readings. Calibration performance for the temperature, pH, turbidity, DO, and depth sensors is summarized in Tables 2-6. Overall, the post-regression results indicate that regression-based compensation improved the agreement between raw sensor output and reference values under the tested calibration conditions.

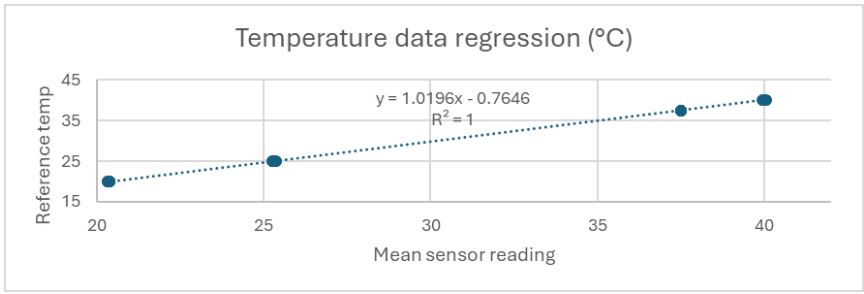

(a) Temperature

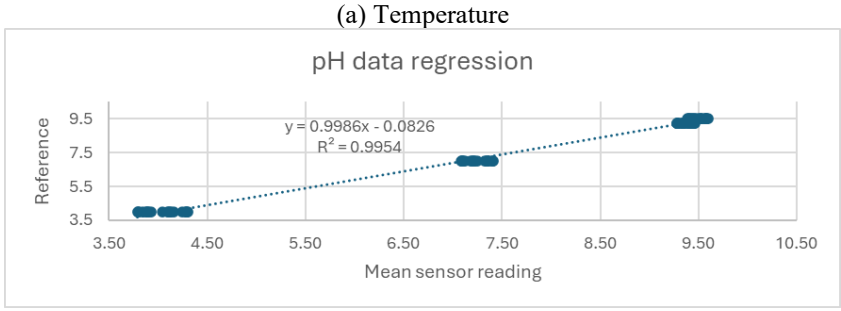

(b) pH

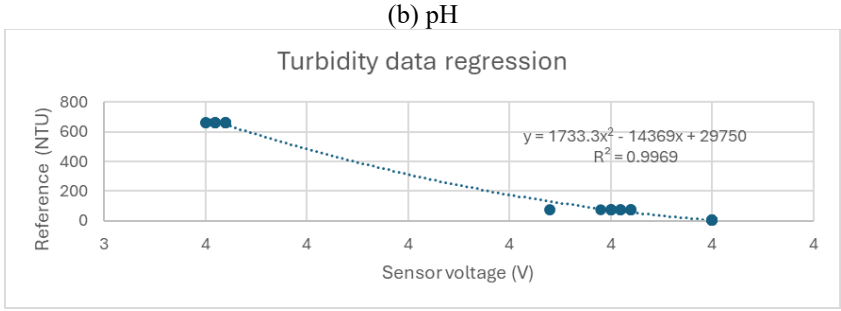

(c) Turbidity

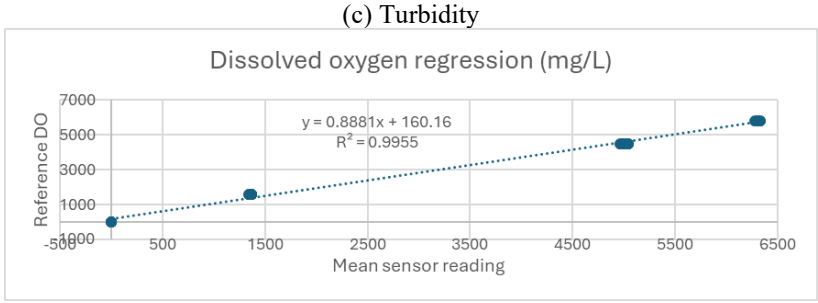

(d) Dissolved Oxygen (DO)

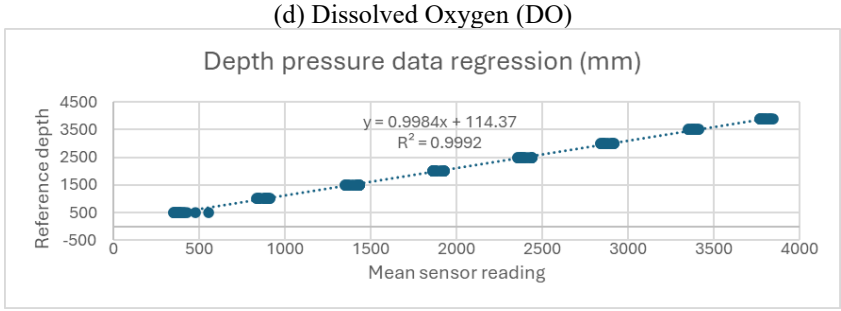

(e) Depth

Figure 9. Calibration regression plots for the measured parameters

Table 2. Temperature sensor calibration and regression

Sample	Reference (°C)	Sensor Mean (°C)	After Regression (°C)	Error Before (%)	Error After (%)
1	20.00	20.34	19.97	1.70	0.13
2	25.00	25.30	25.03	1.20	0.13
3	37.50	37.50	37.47	0.00	0.08
4	40.00	40.00	40.02	0.00	0.05
Mean	-	-	-	0.73	0.10

Table 3. pH sensor calibration and regression

Sample	Reference (pH)	Sensor Means (pH)	After Regression (pH)	Error Before (%)	Error After (%)
1	4.00	4.04	3.95	1.00	1.21
2	7.00	7.24	7.15	3.43	2.10
3	9.26	9.36	9.27	1.10	0.07
4	9.50	9.49	9.40	0.07	1.08
Mean	-	-	-	1.40	1.12

Table 4. Turbidity sensor calibration and regression

Sample	Sensor voltage	Reference (NTU)	After regression (NTU)	Residual (NTU)
1	4.00	3.37	7	3.63
2	3.89	78.00	83	5.00
3	3.50	664.00	669	5.00

Table 5. Dissolved oxygen (DO) sensor calibration and regression

Sample	Reference (mg/L)	Sensor Means (mg/L)	After Regression (mg/L)	Error Before (%)	Error After (%)
1	0.00	0.00	0.16	0.00	1.60
2	1.60	1.36	1.37	15.04	14.53
3	4.50	5.01	4.61	11.31	2.41
4	5.80	6.31	5.76	8.78	0.63
Mean	-	-	-	8.78	4.80

Table 6. Depth (pressure) sensor calibration and regression

Sample	Reference (mm)	Sensor Means (mm)	After Regression (mm)	Error Before (%)	Error After (%)
1	500	394	508	21.22	1.52
2	1000	874	987	12.63	1.33
3	1500	1398	1510	6.81	0.66
4	2000	1888	1999	5.61	0.04
5	2500	2396	2507	4.14	0.28
6	3000	2881	2991	3.95	0.30
7	3500	3381	3490	3.41	0.30
8	3900	3800	3908	2.56	0.22
Mean	-	-	-	7.54	0.58

Representative calibration regressions are shown in Figure 9, illustrating strong fitted relationships between mean sensor readings and reference values across the tested calibration points. The regression plots indicate high goodness of fit for pH, turbidity, depth, and DO, with similarly strong visual agreement for temperature, supporting the use of regression-based correction as the calibration basis for the present prototype.

Among the tested channels, the temperature sensor showed the strongest agreement with its references after compensation, with a mean post-regression error of 0.10%. Across the four tested temperature points, the corrected values remained very close to the reference measurements, indicating stable calibration behavior within the tested range. This result supports the use of the temperature channel for subsequent integrated profiling under controlled conditions.

The pH channel also showed good agreement after regression, with a mean post-calibration error of 1.12%. Across the four tested buffer conditions, the compensated values remained close to the references, indicating that the pH channel was sufficiently stable for controlled prototype operation. Although the pH performance was not as strong as temperature, its residual error remained low enough to support subsequent integrated testing under controlled conditions.

For turbidity, calibration performance is reported using absolute residuals in NTU rather than percentage error because the calibration values are expressed directly in physical turbidity units and only three reference levels were used in the present prototype calibration. Across those tested points, the post-regression residuals were 3.63 NTU, 5.00 NTU, and 5.00 NTU, indicating that the regression reduced deviation to a relatively small range in physical units over the tested operating points. At the same time, the limited number of reference points means that the turbidity calibration should be interpreted as adequate for controlled prototype validation rather than as a broad qualification of the sensor across a wider turbidity range. The present turbidity results are therefore encouraging for controlled prototype use, but they should still be interpreted in light of the broader practical challenges commonly reported for low-cost turbidity sensing in

continuous in-situ applications [15-17].

Among all measured parameters, the DO channel requires the most cautious interpretation. After regression, the mean post-calibration error decreased from 8.78% to 4.80%, showing clear improvement but still remaining the largest residual error among the tested sensors. However, the absolute post-regression deviations are more modest when expressed in physical units: the residuals are approximately 0.16 mg/L at 0.00 mg/L, 0.23 mg/L at 1.60 mg/L, 0.11 mg/L at 4.50 mg/L, and 0.04 mg/L at 5.80 mg/L. This indicates that the percentage error appears relatively high in part because the calibration range includes low-concentration points, where small absolute deviations translate into larger relative error. The remaining DO deviation is also consistent with the greater sensitivity of membrane-based DO measurement to stabilization time, local measurement variability, and settling behavior after probe repositioning. Accordingly, the present DO channel is best interpreted as adequate for indicative profiling under controlled conditions, but not yet as sufficient for resolving very subtle oxygen gradients in strongly stratified natural waters without further validation.

The depth channel also showed strong agreement after regression, with a mean post-regression error of 0.58% over eight reference depths. This indicates that the pressure-based depth channel provided stable calibration behavior across the tested water-column range. Compared with the other measured parameters, the relatively denser depth calibration set strengthens confidence in the pressure-to-depth conversion used later for automated positioning.

Taken together, the calibration results support the use of regression-based compensation for controlled prototype evaluation of the integrated platform. Calibration density was not uniform across the sensing channels, with four reference points for temperature, pH, and DO, three for turbidity, and eight for depth. The present results should therefore be interpreted as adequate for controlled-system testing rather than as full long-term field qualification.

3.2 Controlled multi-depth null-profile test

After calibration, an integrated experiment was conducted in a 4 m deep pool to evaluate the platform's ability to produce coherent multi-parameter measurements at different commanded depths under controlled conditions. The submersible unit was moved to a series of depth setpoints between approximately 0.5 and 4.0 m, and at each setpoint the system recorded temperature, pH, DO, and turbidity. A total of ten measurement sequences were acquired in this experiment. The depth-associated measurement results obtained in this null-profile test are summarized in Table 7.

Across all tested depths, the water column was nearly homogeneous. Temperature varied only from 26.82 ℃ to 26.87 ℃ with a mean of 26.84 ℃, indicating the absence of measurable thermal stratification during the experiment. The measured pH ranged from 6.96 to 7.10 with a mean of 7.02, corresponding to neutral to slightly alkaline conditions. DO remained consistently high, ranging from 8.34 mg/L to 8.89 mg/L with a mean of 8.73 mg/L, while turbidity was low and stable at approximately 5.00 NTU, consistent with visually clear pool water. These results indicate that the test environment did not contain strong vertical gradients in the measured parameters.

The main value of this experiment lies in the internal consistency of the integrated platform under conditions where strong vertical gradients were not expected. Repeated measurements at nominally similar depths, such as the paired observations at 49–50 cm, the repeated trials at 201 cm, and the paired observations at 399–401 cm, remained mutually consistent within the expected sensor uncertainty. This indicates that, in a vertically homogeneous water column, the combined sensing, depth-positioning, data handling, and transmission pipeline does not introduce artificial temperature, pH, DO, or turbidity gradients. In that sense, the experiment functions as a controlled null-profile validation of the end-to-end system rather than as evidence of natural vertical stratification.

Accordingly, this test supports the controlled-environment feasibility of the integrated profiling workflow, but it does not demonstrate the ability of the prototype to resolve thermoclines, hypoxic layers, or turbidity gradients in a truly stratified lake or reservoir. The present experiment should therefore be interpreted as proof that the prototype can acquire and return depth-associated measurements coherently in a homogeneous water column, while field validation in naturally stratified environments remains necessary for broader performance claims. The accuracy of the associated depth-positioning behavior is evaluated separately in Section 3.3.

3.3 Depth-positioning performance

The second integrated experiment evaluated the performance of the automatic depth-positioning mechanism responsible for placing the submersible unit at user-defined depths. The system was commanded through the interface to move to setpoints of 50, 100, 200, 300, and 400 cm. For each setpoint, two repetitions were carried out, and both the pressure-based depth reading and the actual depth measured manually were recorded. The resulting data are summarized in Table 8.

Table 7. Water-quality measurements collected by the system at various depths

Measurement Sequence	Depth (cm)	Temperature (℃)	pH	Dissolved Oxygen (DO) (mg/L)	Turbidity (NTU)
1	49	26.83	7.10	8.83	4.99
2	50	26.82	7.02	8.71	4.99
3	100	26.85	7.08	8.49	4.99
4	99	26.85	6.99	8.34	5.00
5	201	26.82	7.04	8.85	4.99
6	201	26.87	7.03	8.76	5.00
7	301	26.83	6.96	8.88	5.00
8	299	26.85	6.98	8.89	5.00
9	401	26.84	7.01	8.81	5.00
10	399	26.85	6.97	8.72	5.00

Table 8. Depth-control evaluation

Setpoint (cm)	Sensor Reading (cm)	Actual Depth (cm)	Error
50	49	40	10
50	51	42	8
100	100	104	4
100	99	102	2
200	201	203	3
200	201	204	4
300	301	303	3
300	299	301	1
400	401	402	2
400	399	398	2

A clear depth-dependent accuracy pattern was observed. At the shallowest setpoint of 50 cm, the actual depths were 40 cm and 42 cm, corresponding to absolute errors of 10 cm and 8 cm, or approximately 16–20% relative error. In contrast, the errors at deeper setpoints were substantially smaller: 2–4 cm at 100 cm, 3–4 cm at 200 cm, 1–3 cm at 300 cm, and 2 cm at 400 cm. When the eight trials between 100 cm and 400 cm are aggregated, the mean absolute error is approximately 2.6 cm, with a root-mean-square error of about 2.8 cm, corresponding to relative errors on the order of 0.5–3% of the target depth. These results indicate that the positioning mechanism performs more consistently at intermediate and deeper setpoints than near the surface. This depth-dependent trend is consistent with the hydrostatic pressure-difference principle used in the prototype. Depth is estimated from the pressure difference between the sensor on the submersible unit and the reference pressure near the surface, following Eq. (2). At shallow depth, the pressure difference ΔP is still relatively small, so minor fluctuations or pressure-reading uncertainty produce a proportionally larger relative error in the estimated depth. As the submersible unit moves deeper, the pressure difference becomes larger, and the resulting depth estimate becomes more stable. Accordingly, the larger deviations observed at the 50 cm setpoint should be interpreted as a limitation of the present pressure-comparison approach in the near-surface region rather than as a general failure of the positioning mechanism. Secondary contributions may also arise from small mechanical effects such as cable slack, but the limited pressure difference near the surface is considered the main reason for the weaker shallow-depth performance. Under the reported controlled test conditions, the pressure-feedback and stepper-actuated shaft mechanism showed practical positioning accuracy at intermediate and deeper setpoints. However, the present results do not establish uniform profiling precision across the full water column, nor do they demonstrate full operational robustness in natural lake and reservoir environments where waves, currents, and platform motion may further affect the cable-actuation process. Within the scope of this study, the depth-control experiment therefore supports the controlled-environment feasibility of automated multi-depth positioning, while also identifying shallow-depth operation as the weakest regime of the current prototype. This limitation should be considered in interpreting the integrated profiling results and in planning future field-oriented improvements.

3.4 End-to-end IoT data integrity and communication performance

End-to-end IoT performance was evaluated by comparing measurements displayed locally on the device with the corresponding records stored in the cloud database and shown in the Android application. Under the reported test conditions, the numerical values matched to two decimal places across the local display, cloud storage, and mobile interface. This indicates that the acquisition, transmission, storage, and visualization chain preserved the recorded data without observable discrepancy in the tested examples. Representative consistency between the liquid crystal display (LCD), cloud database, and application interface is shown in Figure 10.

This result confirms that the implemented IoT workflow functioned correctly during prototype validation. The agreement between the local display, cloud database, and mobile application shows that the complete command-and-return chain operated as intended under the reported test conditions. In practical terms, Figure 10 demonstrates that requested depth commands could be executed and that the resulting depth-tagged measurements could be returned, stored, and accessed without observable discrepancy in the tested examples.

(a) liquid crystal display (LCD) display data

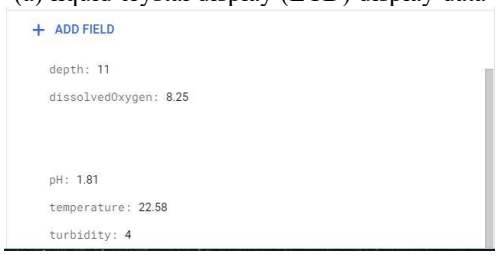

(b) Data on cloud database

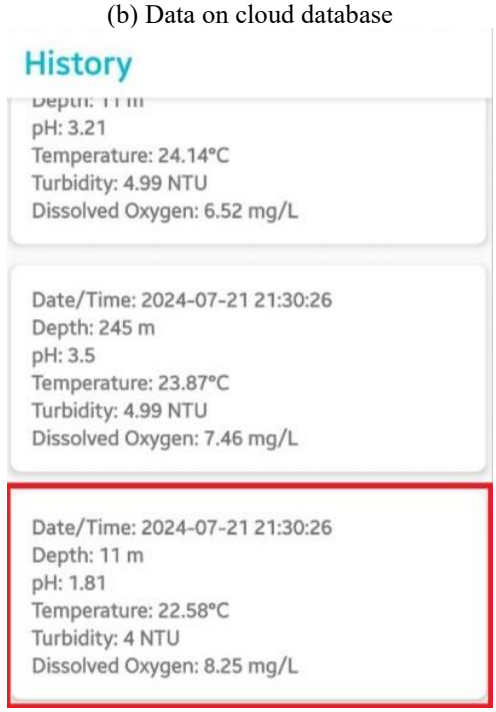

(c) History page of Android application

Figure 10. Data collection and storage

Table 9 complements this end-to-end check by providing

subsystem-level communication results for the LoRa link. Under line-of-sight conditions, the link maintained 0% packet loss up to 70 m, while communication quality degraded at 90 m. Taken together, these results support the controlled-environment feasibility of synchronized cloud logging, mobile access, and moderate-distance LoRa communication. However, reconnection behavior, non-line-of-sight performance, obstruction effects, and broader field communication robustness were not evaluated and remain targets for future validation.

Table 9. LoRa communication performance under line-of-sight subsystem testing

Distance (m)	RSSI (dB)	Delay (ms)	Packet Loss (%)	Result
10	-76.18	501.90	0	Good
20	-83.27	710.36	0	Good
50	-85.00	807.90	0	Good
70	-85.20	921.50	0	Good
90	-90.27	960.54	50	Poor

3.5 Comparative discussion and implications

Table 10 compares the present prototype with selected low-cost water-quality monitoring systems in terms of functional scope rather than matched-condition performance. The cited systems were developed for different monitoring contexts, including point-of-use sensing, surface surveying, long-term autonomous buoy deployment, and offshore aquaculture monitoring. Within that comparison, the present work occupies a different niche by combining a floating supervisory unit, a submersible sensing unit, and IoT-linked data access to support portable depth-associated measurements under controlled 4 m pool validation.

The main contribution of the prototype is therefore not demonstrated superiority over those systems, but extension of low-cost monitoring from surface-only or fixed-point configurations toward depth-aware profiling. In the Indonesian context, this remains relevant because the prototype targets temperature, pH, DO, turbidity, and depth, which are core parameters for inland-water assessment. However, the present evidence supports prototype feasibility rather than operational deployment, and broader practical claims will require real-environment validation.

Table 10. Functional comparison of selected low-cost water-quality monitoring systems

References	Depth Profiling	Main Measured Parameters	Connectivity / User Access	Validation / Deployment Context
[11]	No	pH, free chlorine, temperature, BPA	Bluetooth / smartphone app / cloud-linked app workflow	On-site and point-of-use water testing
[12]	No	pH, temperature, DO, EC, GPS-tagged location	NB-IoT / LTE-M, Bluetooth, cloud visualization	High-frequency short-term surveys in flowing urban or hard-to-access waters
[13]	No	Temperature, pH, DO, EC, turbidity	LoRa / gateway / remote server, plus Bluetooth and Wi-Fi support	Long-term autonomous deployment across multiple surface-water sites
[14]	No	Temperature, DO, salinity, water velocity	LoRa to shore server / mobile app / AI-assisted prediction	Fixed offshore aquaculture deployment near marine cages
This work	Yes (winch-based)	Temperature, pH, DO, turbidity, depth	Cloud database + Android app + LoRa-based link	Controlled 4 m pool prototype validation

3.6 Limitations and future work

The present study should be understood as an initial system-development step toward improving observation of vertical water-quality gradients that are difficult to capture through conventional surface sampling or delayed laboratory analysis. Within that purpose, the prototype has demonstrated that depth-associated measurements can be acquired directly in the water column and returned through an integrated sensing and IoT workflow. However, the current work remains limited to controlled 4 m pool validation, so the results should be interpreted as evidence of prototype feasibility rather than as a final monitoring solution for natural lakes or reservoirs. In addition, because the integrated multi-depth test was carried out in a nearly homogeneous water column, the present study confirms the consistency of the measurement workflow in a null-profile setting but does not yet demonstrate performance in naturally stratified environments.

Accordingly, future work should move from this first-stage prototype toward a more permanent and longer-term inland-water monitoring system. The next development stage should focus on real-environment deployment, improved stability of the weaker sensing and positioning functions, and stronger long-duration operation for field use. In that sense, the current prototype provides a practical foundation for a monitoring approach aimed specifically at resolving depth-dependent water-quality variation more effectively than conventional methods. In a broader sense, this development path is also aligned with the continuing need to strengthen freshwater monitoring capacity and water-quality assessment in practical environmental management [25].

4. CONCLUSION

This study addressed the difficulty of observing vertical water-quality gradients using conventional manual or laboratory-based monitoring by developing a portable depth-aware monitoring prototype that integrates a floating supervisory unit, a submersible sensing unit, and an IoT-based communication layer. The main contribution of the work lies in the engineering integration of direct depth-associated in-situ measurement, automatic vertical positioning, and real-time data handling within a single prototype system. The experimental results support the controlled-environment feasibility of the proposed design. Calibration showed strong post-regression performance for temperature (0.10%), pH (1.12%), and depth (0.58%), while DO remained the weakest channel with a mean post-calibration error of 4.80%. Integrated testing in a 4 m pool produced coherent multi-parameter measurements in a nearly homogeneous water column, confirming the system's ability to acquire depth-

associated data without introducing artificial gradients in a null-profile environment. The depth-positioning test further showed that the 50 cm setpoint was the weakest operating condition, with 8–10 cm error, whereas deeper setpoints between 100 and 400 cm showed substantially smaller deviations. The IoT evaluation confirmed end-to-end consistency between the local display, cloud database, and Android application, while LoRa subsystem testing showed 0% packet loss up to 70 m under line-of-sight conditions. Overall, the present study should be interpreted as a first-step prototype study rather than a field-ready monitoring solution. Nevertheless, it provides a useful foundation for future development toward a more permanent and longer-term inland-water monitoring system capable of better observing depth-dependent water-quality gradients that are difficult to capture through conventional monitoring alone.

ACKNOWLEDGMENT

The authors acknowledge the School of Electrical Engineering and the University Center of Excellence Intelligent Sensing–IoT, Telkom University, for providing laboratory facilities and technical support during prototype development, sensor calibration, and experimental validation.

REFERENCES

[1] Woolway, R.I., Sharma, S., Smol, J.P. (2022). Lakes in hot water: The impacts of a changing climate on aquatic ecosystems. Bioscience, 72(11): 1050-1061. https://doi.org/10.1093/biosci/biac052

[2] Whitehead, P.G., Wilby, R.L., Battarbee, R.W., Kernan, M., Wade, A.J. (2009). A review of the potential impacts of climate change on surface water quality. Hydrological Sciences Journal, 54(1): 101-123. https://doi.org/10.1623/hysj.54.1.101

[3] Delpla, I., Jung, A.V., Baures, E., Clement, M., Thomas, O. (2009). Impacts of climate change on surface water quality in relation to drinking water production. Environment International, 35(8): 1225-1233. https://doi.org/10.1016/j.envint.2009.07.001

[4] Costa, K.M., Russell, J.M., Vogel, H., Bijaksana, S. (2015). Hydrological connectivity and mixing of Lake Towuti, Indonesia in response to paleoclimatic changes over the last 60,000 years. Palaeogeography, Palaeoclimatology, Palaeoecology, 417: 467-475. https://doi.org/10.1016/j.palaeo.2014.10.009

[5] Fukushima, T., Matsushita, B., Subehi, L., Setiawan, F., Wibowo, H. (2017). Will hypolimnetic waters become anoxic in all deep tropical lakes? Scientific Reports, 7(1): 45320. https://doi.org/10.1038/srep45320

[6] Indonesia. (2021). Lampiran VI peraturan pemerintah republik indonesia nomor 22 tahun 2021 tentang penyelenggaraan perlindungan dan pengelolaan lingkungan hidup tentang baku mutu air danau dan sejenisnya. Sekretariat Negara, Jakarta. https://peraturan.bpk.go.id/Details/161852/pp-no-22-tahun-2021.

[7] Marcé, R., George, G., Buscarinu, P., Deidda, M., et al. (2016). Automatic high frequency monitoring for improved lake and reservoir management. Environmental Science & Technology, 50(20): 10780-10794. https://doi.org/10.1021/acs.est.6b01604

[8] Rogora, M., Cancellario, T., Caroni, R., Kamburska, L., et al. (2023). High-frequency monitoring through in-situ fluorometric sensors: A supporting tool to long-term ecological research on lakes. Frontiers in Environmental Science, 10: 1058515. https://doi.org/10.3389/fenvs.2022.1058515

[9] Bratic, G., Carrion, D., Cannata, M., Rogora, M., Strigaro, D., Brovelli, M.A. (2022). Lake water quality monitoring tools developed in the SIMILE project. In the International Archives of the Photogrammetry, Remote Sensing and Spatial Information Sciences, pp. 599-606. https://doi.org/10.5194/isprs-archives-XLIII-B4-2022-599-2022

[10] Rozemeijer, J., Jordan, P., Hooijboer, A., Kronvang, B., et al. (2025). Best practice in high-frequency water quality monitoring for improved management and assessment; a novel decision workflow. Environmental Monitoring and Assessment, 197(4): 353. https://doi.org/10.1007/s10661-025-13795-z

[11] Alam, A.U., Clyne, D., Deen, M.J. (2021). A low-cost multi-parameter water quality monitoring system. Sensors, 21(11): 3775. https://doi.org/10.3390/s21113775

[12] Agade, P., Bean, E. (2023). GatorByte–An internet of things-based low-cost, compact, and real-time water resource monitoring buoy. HardwareX, 14: e00427. https://doi.org/10.1016/j.ohx.2023.e00427

[13] Quevy, Q., Lamrini, M., Chkouri, M., Cornetta, G., Touhafi, A., Campo, A. (2023). Open sensing system for long term, low cost water quality monitoring. IEEE Open Journal of the Industrial Electronics Society, 4: 27-41. https://doi.org/10.1109/OJIES.2022.3233919

[14] Lu, H.Y., Cheng, C.Y., Cheng, S.C., Cheng, Y.H., et al. (2022). A low-cost AI buoy system for monitoring water quality at offshore aquaculture cages. Sensors, 22(11): 4078. https://doi.org/10.3390/s22114078

[15] Droujko, J., Molnar, P. (2022). Open-source, low-cost, in-situ turbidity sensor for river network monitoring. Scientific Reports, 12(1): 10341. https://doi.org/10.1038/s41598-022-14228-4

[16] Gillett, D., Marchiori, A. (2019). A low-cost continuous turbidity monitor. Sensors, 19(14): 3039. https://doi.org/10.3390/s19143039

[17] Wang, M., Shi, B., Catsamas, S., Kolotelo, P., McCarthy, D. (2024). A compact, low-cost, and low-power turbidity sensor for continuous in situ stormwater monitoring. Sensors, 24(12): 3926. https://doi.org/10.3390/s24123926

[18] Sahu, N., Maldhure, A. (2025). Framework for evaluating the performance of water quality sensors. Cleaner Water, 4: 100144. https://doi.org/10.1016/j.clwat.2025.100144

[19] Naloufi, M., Abreu, T., Souihi, S., Therial, C., et al. (2024). Long-term stability of low-cost IoT system for monitoring water quality in urban rivers. Water, 16(12): 1708. https://doi.org/10.3390/w16121708

[20] Pérez-López, C.A., Pantoja, W., Pérez-Taborda, J.A., Ávila, A. (2023). PortAqua: A low-cost, compact water quality meter for science communication. Environmental Monitoring and Assessment, 195(2): 336. https://doi.org/10.1007/s10661-022-10804-3

[21] Chapman, D.V. (2021). Water Quality Assessments: A Guide to the Use of Biota, Sediments and Water in

Environmental Monitoring. CRC Press. https://doi.org/10.1201/9781003062103
[22] Bartram, J., Ballance, R. (1996). Water Quality Monitoring: A Practical Guide to the Design and Implementation of Freshwater Quality Studies and Monitoring Programmes. CRC Press.
[23] Flores-Iwasaki, M., Guadalupe, G.A., Pachas-Caycho, M., Chapa-Gonza, S., Mori-Zabarburú, R.C., Guerrero-Abad, J.C. (2025). Internet of Things (IoT) sensors for water quality monitoring in aquaculture systems: A systematic review and bibliometric analysis. AgriEngineering, 7(3): 78. https://doi.org/10.3390/agriengineering7030078
[24] Shete, R.P., Bongale, A.M., Dharrao, D. (2024). IoT-enabled effective real-time water quality monitoring method for aquaculture. MethodsX, 13: 102906. https://doi.org/10.1016/j.mex.2024.102906
[25] Coordination, U.N.E.P. (2016). A Snapshot of the World's Water Quality: Towards a Global Assessment. Nairobi, United Nations Environment Programme.

NOMENCLATURE

F_b	buoyant force, N
F_{net}	net submerged force, N
g	gravitational acceleration, $m \cdot s^{-2}$
h	estimated depth, m
m	submersible-unit mass, kg
r	effective shaft radius, m
T	shaft torque, N·m
V	displaced volume, m^3
W	dry weight of submersible unit, N
l	length of submersible unit, m
w	width of submersible unit, m
H	height of submersible unit, m

Greek symbols

ΔP	pressure difference, Pa
r	water density, $kg \cdot m^{-3}$

Subscripts

b	buoyant
net	net submerged